RESEARCH PAPER

Potassium triiodide-quenched gold nanocluster as a fluorescent turn-on probe for sensing cysteine/homocysteine in human serum

John Nebu [1] · J. S. Anjali Devi [1] · R. S. Aparna [1] · B. Aswathy [1] · G. M. Lekha [1] · George Sony [1]

Abstract

A fluorescent sensing platform using KI_3-quenched bovine serum albumin stabilized gold nanoclusters has been designed and used as a fluorescent probe for the turn-on detection of homocysteine/cysteine (Cys/Hcy). The fluorescence of gold nanoclusters was quenched by iodine. The fluorescence of quenched gold nanoclusters was effectively switched on by Cys/Hcy devoid of the interference of glutathione. The transmission electron microscopy image, X-ray photoelectron spectroscopy analysis, time-correlated single photon counting analysis, and dynamic light scattering data confirmed the aggregation-induced quenching of fluorescence of gold nanoclusters by iodine. The turn-on response of Cys/Hcy shows two linear ranges from 0.0057 to 5 μM and from 8 to 25 μM, with a limit of detection of 9 nM for cysteine and 12 nM for homocysteine. Real samples were analyzed to monitor Cys/Hcy added to human serum. The fluorescence turn-on response of the probe on a paper strip in the presence of Cys/Hcy was studied.

Keywords Gold nanocluster · Fluorescence turn on · Cysteine · Homocysteine · Bovine serum albumin · Iodine

Introduction

Clinicians have recognized homocysteine (Hcy) as a potential biomarker for cardiovascular disease, chronic kidney disease, and diabetes [1, 2]. Epidemiologic studies of mental illness in children and adolescents have shown that elevated Hcy levels are associated with anxiety and depression [3]. Hcy is a thiol-containing amino acid, an intermediate of methionine synthesis, which is involved in transmethylation and plays a major role in maintaining the proper functioning of the central nervous system [4]. Poor dietary intake of folic acid, vitamin B_{12}, and vitamin B_6 and reduced enzymatic activities decrease catabolism of Hcy and result in increase in the intracellular Hcy concentration [5, 6]. The elevation of Hcy levels beyond normal levels in the blood (hyperhomocysteinemia) is associated with stroke, heart attack, and blood clot formation (thrombosis) [7]. Hyperhomocysteinemia is linked to renal failure as well as diabetes [8, 9].

The metabolic pathway for the conversion of Hcy to methionine or cysteine (Cys) involves the transfer of a methyl group to the protein (see the electronic supplementary material), and from this it is clear that if Hcy is not converted into methionine or Cys, its levels will increase in blood plasma or serum [10]. Therefore, it is essential to develop a probe for the determination of Hcy/Cys. Currently used analytical methods for the determination of biothiols include high-performance liquid chromatography, capillary electrophoresis, spectrophotometry, mass spectrometry, gas chromatography–mass spectrometry with isotopic dilution, ion-exchange chromatography, voltammetry, and enzymatic methods [11, 12]. Each of these techniques has many advantages as well as disadvantages. In this scenario, a point-of-care strategy for onsite sensing of Hcy is important. Fluorescence-based methods have some advantages over these techniques, such as high sensitivity, cost-effectiveness, speed, and simple operational procedures [13]. Among the fluorescent probes, only a few can discriminate the main thiols such as glutathione, Cys, and Hcy. In the human body, glutathione is more abundant than Cys and Hcy, and

---

✉ George Sony
emailtosony@gmail.com

[1]   Department of Chemistry, School of Physical and Mathematical Sciences, University of Kerala, Kariavattom, Trivandrum, Kerala 695581, India

hence it significantly interferes with Cys and Hcy determination [14]. In this context, it is essential to develop a sensor for "Cys sisters" devoid of interference of glutathione and to identify whether a patient has deficiency regarding Cys/Hcy metabolism.

Researchers have focused on the fluorescent sensing of Cys/Hcy based on nanoparticles as well as organic frameworks. Liu et al. [15] developed a sensor for ratiometric fluorescent detection of Cys. Wu et al. [16] studied the sensing of Cys and Hcy using BODIPY dyes. Yue et al. [17] studied a coumarin-based pH-dependent fluorescent probe for sensing Cys and Hcy. Apyari et al. [18] studied gold-nanoparticle-based sensing of Cys. Sun et al. [19] studied an integrated logic gate for fluorescence turn-on detection of Cys and histidine. Rusin et al. [20] studied the visual detection of Cys and Hcy with a xanthene dye [20]. Yue et al. [21] developed a coumarin-derivative-based fluorescent probe for the detection of Cys and its metabolite SO_2. Liu et al. [22] studied the selective fluorescent detection of Cys in living cells through a Michael addition reaction with an isomer of a 1,8-naphthalimide derivative. Yue et al. [23] developed a turn-on fluorescent probe for the detection of Cys based on thiol–chromene click chemistry . Liu et al. [24] designed a near-infrared sensitive probe based on a squaraine for the detection of Cys/Hcy. Li et al. [25] developed a maleimide-group-based fluorescent probe for the selective detection of biothiols in dimethyl sulfoxide–N-(2-hydroxyethyl)piperazine-N'-ethanesulfonic acid solution.

The fluorescence properties of bovine serum albumin (BSA)-stabilized gold nanoclusters (Au NCs) have been a powerful tool for imaging, sensing, and biolabeling because of their advantages such as biocompatibility, long lifetime, enhanced fluorescence, cost-effectiveness, and nanometer size [26]. BSA can play a dual role as a reductant and a stabilizer for the synthesis of Au NCs, which can act as a robust template to maintain biocompatibility and reduced size [27]. The fluorescence properties of Au NCs have been widely used in the detection of biomolecules such as alkaline phosphatase [28] and cholesterol [29] and in bioimaging applications in cancer cells such as HeLa cells [30] and PANC-1 cells [31]. The fluorescence properties of Au NCs can be selectively quenched by iodine [32].

In this work, BSA-stabilized Au NCs were successfully synthesized, and the Au NCs were quenched by addition of KI_3 (I_2 + KI); the complexes were used as a probe for turn-on sensing of Cys/Hcy (Fig. 1). Real samples were used for the detection of Cys/Hcy in blood serum. The results showed that KI_3-quenched AuNCs (Au NCs@KI_3) can quantitatively detect Cys/Hcy with good selectivity and sensitivity. Moreover, the fluorescence turn-on response of the probe toward Cys and Hcy was successfully evaluated on a paper strip.

Experimental

Materials

All chemicals were of analytical reagent grade or better. Hydrogen tetrachloroaurate trihydrate ($HAuCl_4 \cdot 3H_2O$), Cys, Hcy, arginine, ascorbic acid, aspartic acid, glutamic acid, glycine, histidine, leucine, lysine, methionine, proline, serine, tyrosine, valine, and glutathione were purchased from Alfa Aesar. BSA was obtained from Sigma-Aldrich. Other chemicals were obtained from TCI Chemicals. Millipore water was used in all experiments.

Synthesis of Au NCs

Au NCs were synthesized by the reduction of $HAuCl_4$ with BSA based on a modification of a previously reported method [27]. Briefly, about 250 mg BSA was dissolved in 5 mL water, and 5 mL of 10 mM $HAuCl_4$ was added dropwise with continuous stirring (600 rpm) at ambient temperature. After 2 min, about 0.5 mL of 1 M NaOH was added dropwise so that the color of the solution became pale yellow. The solution was stirred (600 rpm) for 5 min, and heated in a domestic microwave oven at 500 W for about 50 s. The formation of Au NCs was indicated by the change of color of the solution to deep brown with the emission of a deep red color on UV irradiation at 365 nm. The concentration of the synthesized Au NCs was estimated to be approximately 0.02 M [29], and this solution was stored at 4 °C for further use.

Detection procedure

To optimize the ratio of I_2 to KI in KI_3, 3 mL of the synthesized Au NCs was mixed with different amounts of KI_3 sequentially with I_2-to-KI ratios of 1:2, 1:4, and 1:6. The mixture was shaken well, and was equilibrated for 5 min to measure the fluorescence spectra with an excitation wavelength of 480 nm. To obtain the Stern–Volmer plot, 3 mL of the synthesized Au NCs was mixed with different amounts of KI_3 (I_2 to KI ratio 1:6) to get an effective I_2 concentration of 0.05–50 μM.

To analyze the effect of pH, the pH of the synthesized Au NCs (pH 10.4) was adjusted with 0.1 M NaOH and 0.1 M HCl. After analysis, the optimized pH of the synthesized Au NCs was selected for further detection.

To investigate the detection selectivity, 14 different amino acids, ascorbic acid and glutathione—the major thiol-containing interfering agent in human blood—at the same concentration of 25 μM were individually studied. To evaluate and eliminate the possibility of fluorescence quenching created by volume dilution during the addition of the analyte, a blank experiment was conducted by our adding an equivalent amount of Millipore water.
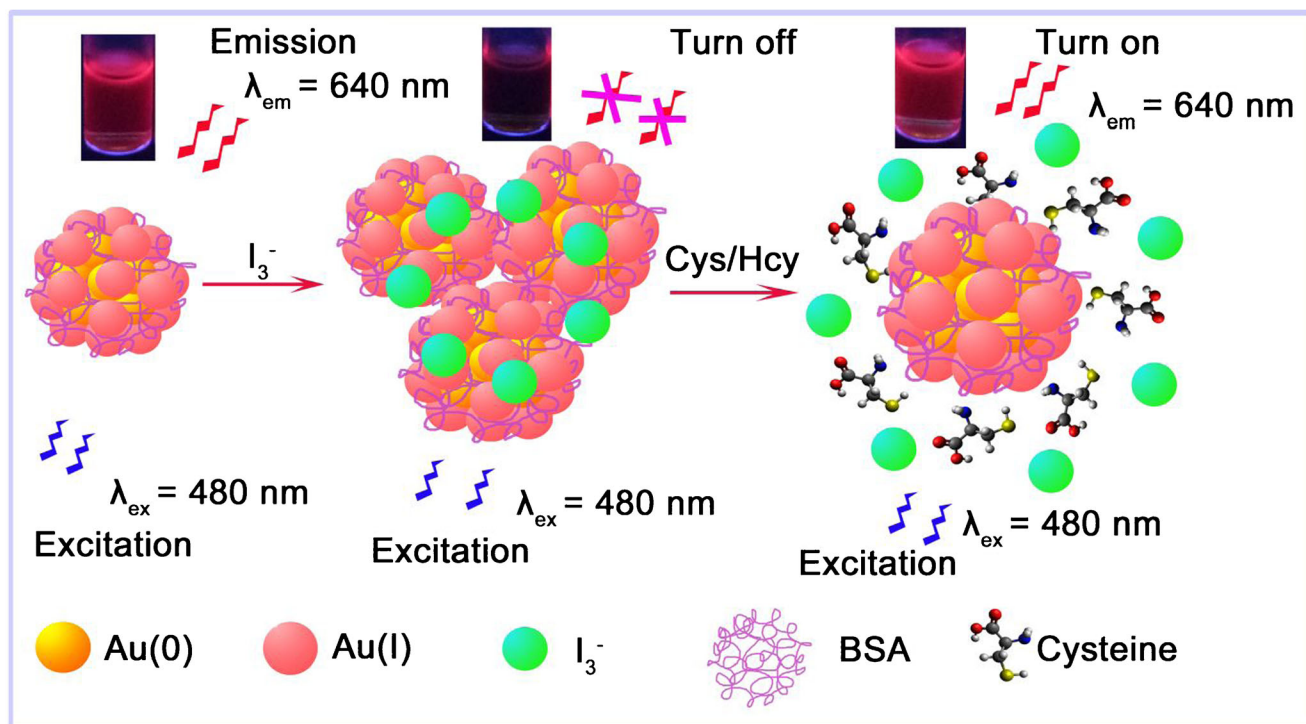
Fig. 1 The mechanism of sensing cysteine (Cys)/homocysteine (Hcy). I_2 induces S–S bond formation between gold nanoclusters (Au NCs) and results in turn off of fluorescence via aggregation. The thiol groups present in pristine Cys/Hcy break the S–S bond between Au NCs and switch on the fluorescence. BSA bovine serum albumin

To detect Cys/Hcy, 3 mL of the synthesized Au NCs (pH 10.4) was mixed with KI_3 (effective concentration of I_2 4 μM). The mixture was shaken thoroughly and equilibrated for 2 min. About 20 μL of different concentration of Cys/Hcy (effective concentration of Cys/Hcy ranging from 0 to 50 μM) was then added, and the mixture was further shaken well, and equilibrated for 2 min before measurement of fluorescence spectra. The time-dependent changes of the fluorescence of the probe in the presence of Cys/Hcy (effective concentration 25 μM) were also studied.

The sensitivity of Cys/Hcy was studied with 12 different amino acids, ascorbic acid, glutathione, and cumulative addition of all amino acids, ascorbic acid and glutathione. In brief, 3 mL of the synthesized Au NCs was mixed with KI_3 (effective concentration of I_2 4 μM), and the mixture was shaken thoroughly. After equilibration for 2 min, it was treated with 12 different amino acids, ascorbic acid and glutathione separately, and 12 different amino acids, ascorbic acid and glutathione together (effective concentration of each amino acid, ascorbic acid and glutathione are 25 μM). Cys and Hcy were then added separately (effective concentration 25 μM).

Detection of Cys/Hcy in human serum

Human serum was collected from healthy volunteers during the morning, and spiked with Cys and Hcy separately. Informed consent was obtained from all individual participants included in the study. Three milliliters of synthesized Au NCs was mixed with 20 μL of different concentrations of Cys- and Hcy-spiked human serum, and the fluorescence spectra were recorded.

### Distinctive response of Cys/Hcy

For the distinctive detection of Cys and Hcy, the turn-on fluorescence response of both amino acids with different concentrations at pH 7.2 was studied.

Results and discussion

Characterization of Au NCs

The BSA-capped Au NCs were synthesized in a one-step process by reduction of Au^{3+} ions to a Au(0)–Au(I) core–shell structure with use of BSA, which also acts as a protecting agent. The absorption spectrum of $HAuCl_4$ shows strong absorption at 295 nm, and the absence of the characteristic surface plasmon peak at 530 nm in the absorption spectrum of Au NCs attests the exclusive conversion of $HAuCl_4$ to Au NCs only and not gold nanoparticles (Fig. 2a) [33]. The BSA-capped Au NCs exhibit fluorescence at 640 nm for excitation at 480 nm (inset in Fig. 2a). The mechanism underlying the fluorescence of Au NCs is attributed to the intrinsic

Fig. 2 a The UV–visible absorption spectra of HAuCl$_4$ and gold nanoclusters (Au NCs). The inset shows the excitation (Ex) and emission (Em) spectra of Au NCs; there is intense red fluorescence of Au NCs on UV illumination at 365 nm. b Transmission electron microscopy image of Au NCs
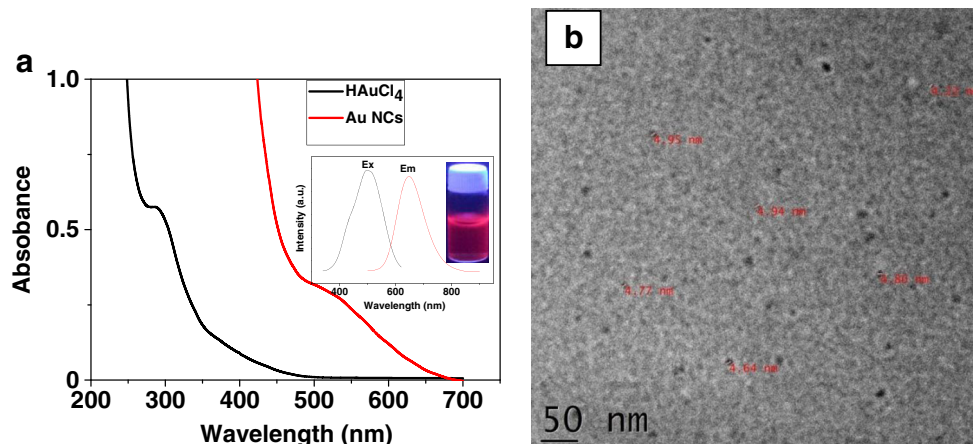
quantization effect within the Au(0) core facilitated by the interaction between the metal core and surface ligands [34]. The BSA-stabilized Au NCs exhibit intense red fluorescence on UV illumination at 365 nm (inset in Fig. 2a). The high-resolution transmission electron microscopy (TEM) image was used to understand the morphology of Au NCs, and reveals a large number of monodisperse Au NCs with an average diameter of approximately 4.0 ± 0.5 nm (Fig. 2b) [35]. Dynamic light scattering (DLS) measurements of Au NCs indicate that the Au NCs have a hydrodynamic diameter of 18.0 ± 2.0 nm, which is because of the hydrophilic nature of BSA (see Fig. S2a) [36].

Quenching of Au NCs with KI$_3$

The fluorescence intensity of Au NCs on treatment with KI$_3$ (I$_2$ + KI) undergoes quenching. The quenching effect of KI$_3$ was studied with I$_2$ and KI in different molar ratios (1:2, 1:4, 1:6) (see Fig. S1). On increase of the concentration of KI, the trend in the plot of fluorescence intensity against concentration of I$_2$ shows that the quenching effect increases [37] (Fig. 3a). It reveals that the best quenching is obtained for an I$_2$-to-KI ratio of 1:6. When the the concentration of I$_2$ is increased but the concentration of KI is kept constant, volatilization of I$_2$ occurs. Here the I$_3^-$ ion formed adsorbs on the Au(0)–Au(I) corona and neutralizes the stabilizing +1 charge residing over Au NCs, leading to the aggregation-induced growth of Au NCs beyond the fluorescence framework of cluster dimensions.

The intense red fluorescence of Au NCs (inset in Fig. 3b) results from the core–shell-like structure, where the Au(0) core is surrounded by a Au(I) corona, which is stabilized by 32 Cys residues present in BSA. The fluorescence of Au NCs is fully quenched with 50 μM I$_2$ (I$_2$-to-KI ratio 1:6) as shown in Fig. 3b and the photographs showing fluorescence of HAuCl$_4$, AuNCs, and Au NCs@KI$_3$ in the inset in Fig. 3b. As indicated in Fig. 3b, 50 μM effective concentration of I$_2$ (I$_2$-to-KI ratio 1:6) induces approximately 97% quenching of the initial fluorescence intensity and 4 μM I$_2$ (I$_2$-to-KI ratio 1:6) induces

approximately 50% quenching. After optimization of the concentration of KI$_3$ for turn-on studies, 4 μM KI$_3$ was used in the sensing probe as a quenched off state for further turn-on studies. Figure 3c shows a plot of relative fluorescence intensity (I_0/I) at 630 nm as a function of I$_2$ concentration. It is clear that the calibration curve has a linear range from 0.05 to 4 μM (I_0/I = 0.1973[I$_2$] + 1.034, R^2 = 0.993), on the basis of a signal-to-noise ratio of 3 (inset in Fig. 3c). Stern–Volmer studies were conducted on the quenching phenomenon, and the plot has a Stern–Volmer constant K_{SV} of 0.1973. Both TEM analysis and DLS analysis were used to obtain structural information on Au NCs@KI$_3$. As shown in Fig. 3d, the AuNCs@KI$_3$ are spherical and uniformly distributed with an average diameter of 63.0 ± 5.0 nm. The DLS measurements indicate that the particles are polydisperse with a mean diameter of 12.9 ± 3.6 nm and 55.1 ± 22.0 nm. The existence of two different hydrodynamic diameters indicates the formation of an aggregated complex and the presence of unreacted Au NCs. It can be attributed to the aggregation-induced quenching of Au NCs through charge neutralization by KI$_3$ (see Fig. S2b).

Selectivity studies

The as-prepared Au NCs@KI$_3$ were treated with 14 different amino acids, ascorbic acid and glutathione—the major interfering biomolecule in human blood—and the fluorescence intensity ratios (I/I_0 at 630 nm) in the absence and presence of 25 μM concentration of different amino acids, 25 μM ascorbic acid 25 μM glutathione, and water were recorded. As shown in Fig. 4, it is clear that only Cys and Hcy can recover the fluorescence of KI$_3$-quenched Au NCs, whereas other coexisting amino acids and glutathione do not elicit any turn-on response for the Au NCs@KI$_3$ system. Glutathione is a tripeptide, in which the thiol group is present in the middle of the molecule. As a result, the reactivity of glutathione is hindered by the steric effect of the thiol group [38]. On the other hand, methionine contains a sulfur atom but it is not in the form of a thiol group and hence lacks reactivity. It is found that with the addition of water as well as cumulative
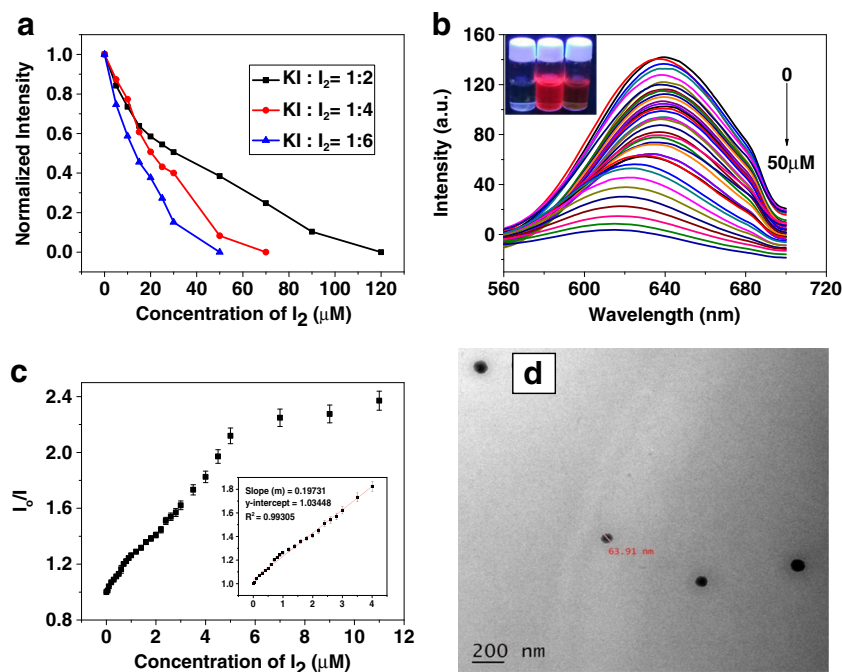
Fig. 3 **a** The variation in the fluorescence intensity of gold nanoclusters (Au NCs) with different concentration ratios of I_2 and KI. **b** Fluorescence spectra of Au NCs in the presence of different concentrations of I_2 and KI (KI_3) (from top to bottom, the concentration of I_2 is from 0 to 50 μM). The inset contains a photograph showing the fluorescence response of $HAuCl_4$, Au NCs, and quenched Au NCs (from left to right). **c** Relative
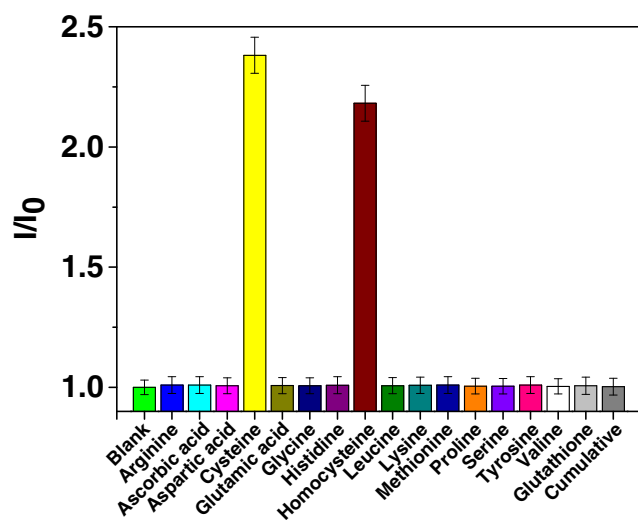
fluorescence intensity (I_0/I at 630 nm) of Au NCs with different concentrations of I_2 (from 0 to 11 μM). The inset shows a Stern–Volmer plot revealing the fluorescence quenching effect on Au NCs from the addition of different concentrations of KI_3 (concentration of I_2 ranging from 0 to 4 μM). **d** Transmission electron microscopy image of Au NC–KI_3

addition of amino acids other than Cys and Hcy the Au NCs@KI_3 system remains in the quenched state.

pH studies

The Cys/Hcy sensing ability of the quenched Au NCs@KI_3 probe at different pH values was investigated (Fig. 5). The Au

Fig. 4 Fluorescence intensity ratios (I/I_0 at 630 nm) of the gold nanocluster (Au NC)–KI_3 ensemble on the addition of different amino acids ascorbic acid and glutathione of concentration 25 μM

NCs@KI_3 are stable within a pH range from 6.0 to 10.5, and their response toward Cys/Hcy remains effective within this pH range (Fig. 5c). The intensity of turn-on fluorescence of Au NCs@KI_3 on addition of Cys/Hcy increases with increase in pH, reaches a maximum at pH 10.4, and then decreases. We selected the solution with pH 10.40 as the solution for further studies. Although the fluorescence intensity slightly decreases with increasing acidity, there is a slight difference in the fluorescence turn-on intensity between Cys and Hcy at pH 7.21. It arises as a result of the difference in the isoelectric point (pI 5.02 for Cys and pI 5.65 for Hcy) between Cys and Hcy, which may be predominant at neutral pH (7.21).

Turn-on sensing of Cys/Hcy

The fluorescence turn-on detection of Cys/Hcy at pH 10.40 was studied with Au NCs@KI_3. As shown in Fig. 6a and c, with increasing concentration of Cys/Hcy (0–50 μM), the fluorescence intensity of Au NCs@KI_3 increases gradually, and when the concentration of Cys/Hcy reaches 50 μM, the fluorescence of Au NCs@KI_3 reaches a maximum, which is greater than the intensity of virgin Au NCs. This happens because the stability of Au NCs is due to the thiol groups of the Cys residue present in BSA [27], which increases further on increase of the concentration of pristine Cys/Hcy. The relative intensity (I/I_0) as the ratio of the fluorescence intensity

Fig. 5 Photographs showing the fluorescence response of KI3-quenched gold nanoclusters (Au NCs) on addition of **a** Cys and **b** Hcy at different pH values. **c** The relative turn-on fluorescence intensity of Au NCs at different pH values (pH from 6 to 10.6)
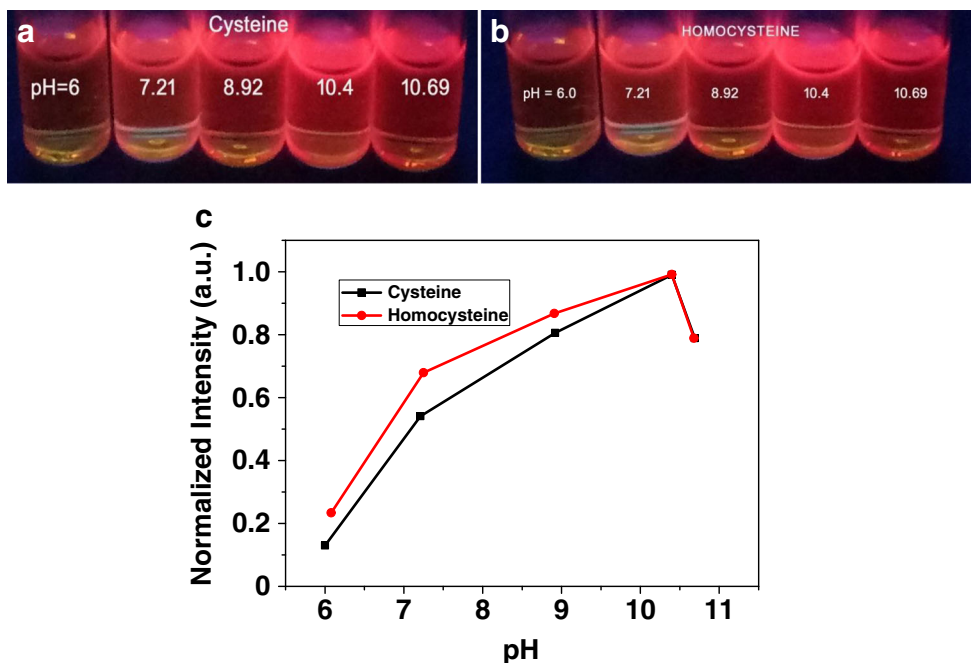
Fig. 6 **a** Fluorescence spectra of the gold nanocluster (Au NC)–KI$_3$ probe on addition of different concentrations of cysteine (from bottom to top, concentration of cysteine ranging from 0 to 50 μM). **b** Relative fluorescence intensity (I/I_0 at 630 nm) of the Au NC–KI$_3$ system against the concentration of cysteine. The inset shows the I/I_0 plot of the Au NC–KI$_3$ system against the concentration of cysteine (8–25 μM). **c** Fluorescence spectra of the Au NC–KI$_3$ system on addition of different concentrations of homocysteine (from bottom to top, concentration of homocysteine ranging from 0 to 50 μM). **d** Relative fluorescence intensity (I/I_0 at 630 nm) of the Au NC–KI$_3$ system against the concentration of homocysteine. (The inset shows the I/I_0 plot of the Au NC–KI$_3$ system against the concentration of homocysteine (8–25 μM). **e** Transmission electron microscopy image of Au NC–KI$_3$. **f** UV–visible absorption spectra of HAuCl$_4$, Au NCs, KI$_3$-quenched Au NCs, and KI$_3$-quenched Au NCs with cysteine
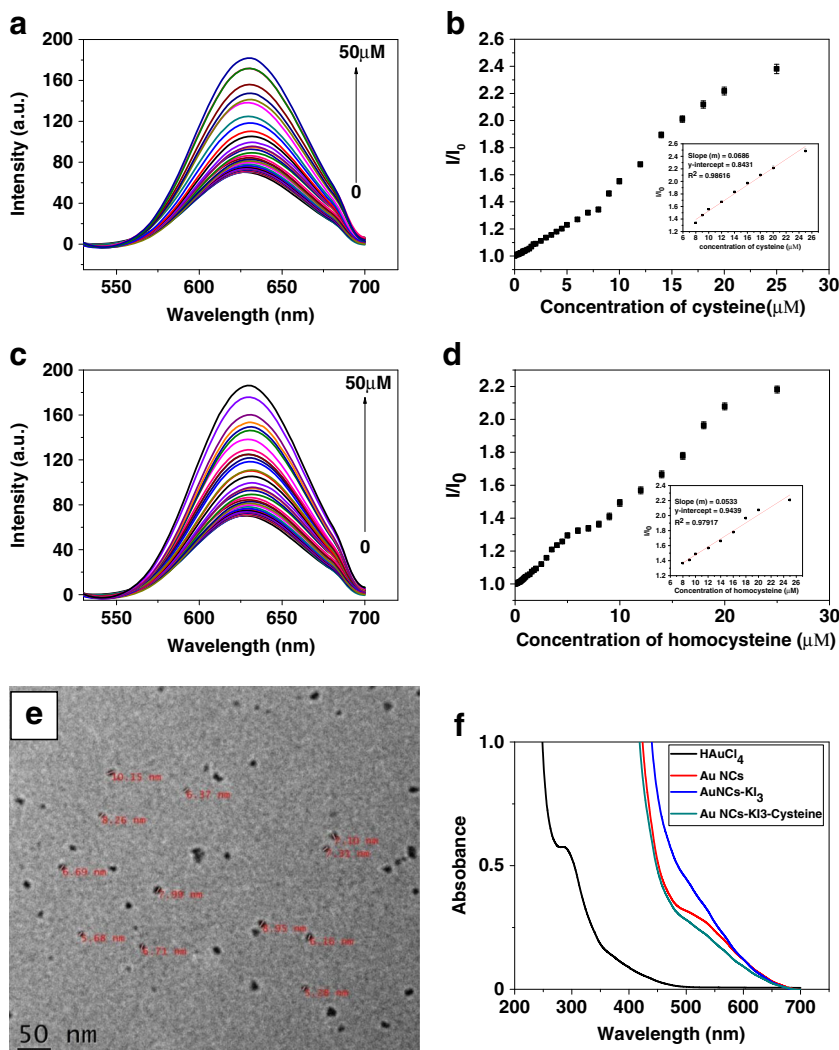
between Au NCs@KI$_3$ and Au NCs@KI$_3$@Cys/Hcy shows a sigmoid curve (Fig. 6b, d) with a linear range from 8 to 25 μM ($I/I_0 = 0.0686$[Cys] $+ 0.8431$, $R^2 = 0.98616$ and $I/I_0 = 0.0533$[Hcy] $+ 0.9439$, $R^2 = 0.97917$). The relative intensity shows another linear range from 0.0057 to 5 μM, with a limit of detection of 9 nM for Cys and 12 nM for Hcy (see Fig. S3).

The high-resolution TEM image of Au NCs@KI$_3$@Cys/Hcy (Fig. 6e) shows that the turn-on ensemble has a diameter of 7.37 $\pm$ 2.5 nm, which indicates the recovery of fine structure of Au NCs, which arises because of the affinity of the thiol groups of Cys/Hcy for Au NCs. The hydrodynamic diameter of Au NCs@KI$_3$@Cys/Hcy was obtained by DLS measurements as 17.7 $\pm$ 3.7 nm, which is ascribed to the less hydrophilic nature of Cys/Hcy as compared with BSA. The UV–visible absorption spectrum of Au NCs@KI$_3$@Cys/Hcy has no surface plasmon resonance peak and has retained the characteristic shoulder peak of Au NCs, which is attributed to the turn-on response of the quenched nanocluster.

The time-dependent changes of fluorescence of Au NCs@KI$_3$@Cys and Au NCs@KI$_3$@Hcy show that the Cys and Hcy enhance the turn-on nature up to 1 h and then have no further effect (see Fig. S4). This indicates the ability of the thiol-containing pristine Cys and Hcy to enhance the turn-on fluorescence of the probe.

Interference studies

To investigate the sensitivity of Au NCs@KI$_3$, Cys and Hcy were analyzed in the presence of different amino acids, ascorbic acid and glutathione (Fig. 7). The coexisting amino acids, ascorbic acid and glutathione with Cys and Hcy proves that the turn-on response of Cys/Hcy remains unperturbed. Moreover, the turn-on response of the probe toward Cys and Hcy in the cumulative presence of all the amino acids, ascorbic acid and glutathione was studied. It was found that the fluorescence turn-on

response of the probe remains intact in the cumulative presence of all the amino acids, ascorbic acid and glutathione.
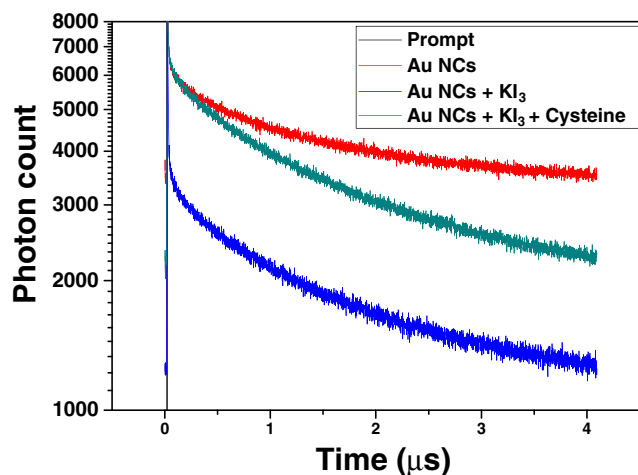
Time-correlated single photon counting analysis

The fluorescence lifetime of Au NCs excited at 330 nm was determined by time-correlated single photon counting (TCSPC) analysis and was found to have triexponential behavior (see Table S1). The fluorescence lifetime is estimated to be about 1.58 μs, and this relatively long fluorescence lifetime arises from the the predominant slow component (94.32%) derived from triplet formation of the Au(0)–Au(I) core-shell structure (Fig. 8). The photostability of Au NCs kept at 4 °C was monitored for about 45 days, and it was found that the intensity of Au NCs is retained in this condition. The fluorescence quenching of Au NCs in the presence of KI$_3$ was studied by life-time analysis with TCSPC as shown in Fig. 8. The fluorescence decay curve retained the triexponential pattern but an obvious decrease in the average lifetime of Au NCs to 1.15 μs occurs after the addition of KI$_3$. The TCSPC analysis of Au NCs@KI$_3$@Cys/Hcy as shown in Fig. 8 indicates that the lifetime of the turn-on ensemble is about 1.49 μs, owing to the recovery of fluorescence in pristine Au NCs [39]. The relative amplitudes of the other two lifetime components are small, but they also contribute somewhat to the average lifetime of Au NCs, Au NCs@KI$_3$, and Au NCs@KI3@Cys/Hcy.

Plausible mechanism

The fluorescence response of Au NCs, Au NCs@KI$_3$, and Au NCs@KI$_3$@Cys/Hcy as shown in Fig. 9a in the solution phase and in a paper strip clearly indicates the quenching of Au NCs by KI$_3$ and fluorescence recovery in the presence of Cys and Hcy. The absence of overlap of the absorption
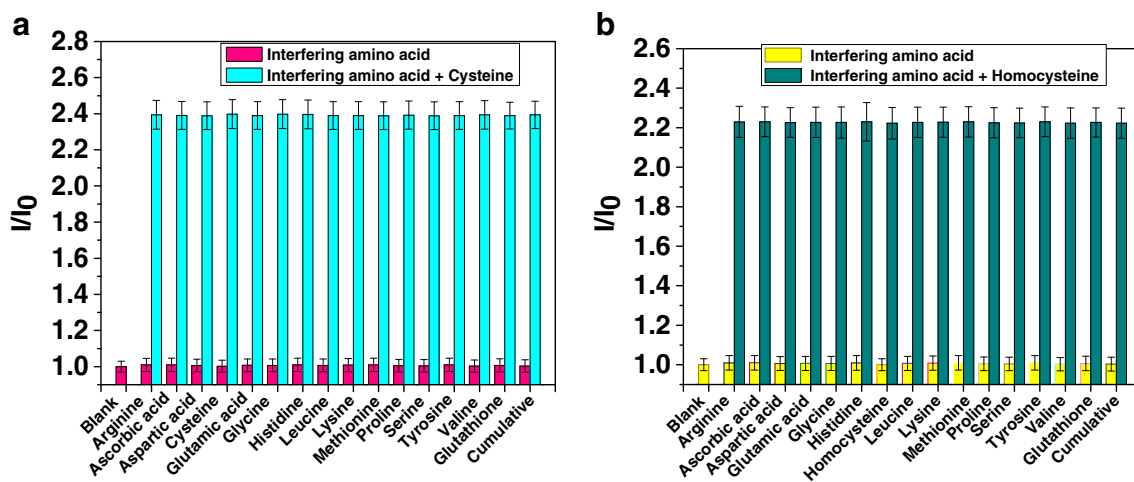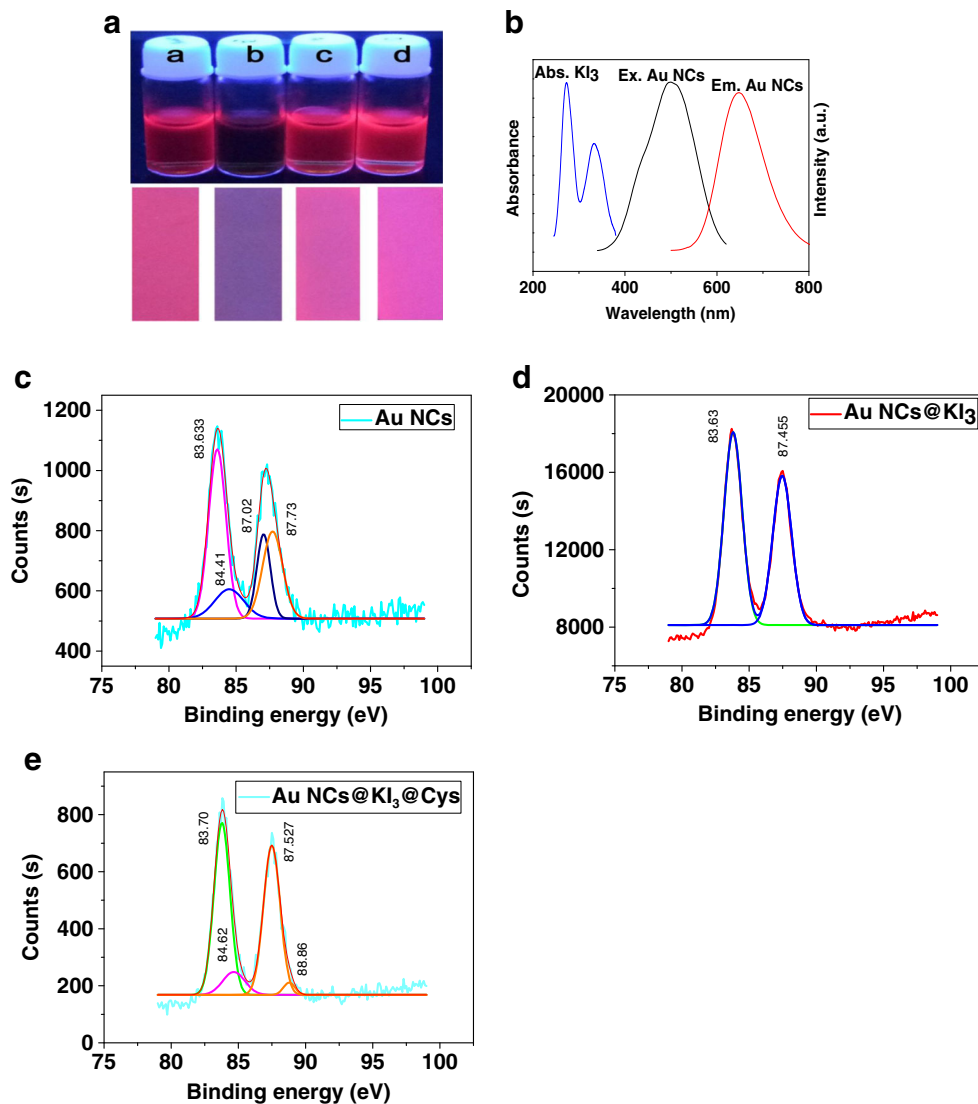

Fig. 7 Fluorescence intensity ratios (I/I_0 at 630 nm) of gold nanoclusters on the addition of different different amino acids, ascorbic acid and glutathione at a concentration of 25 μM and subsequent addition of **a** cysteine (25 μM) and **b** homocysteine (25 μM)
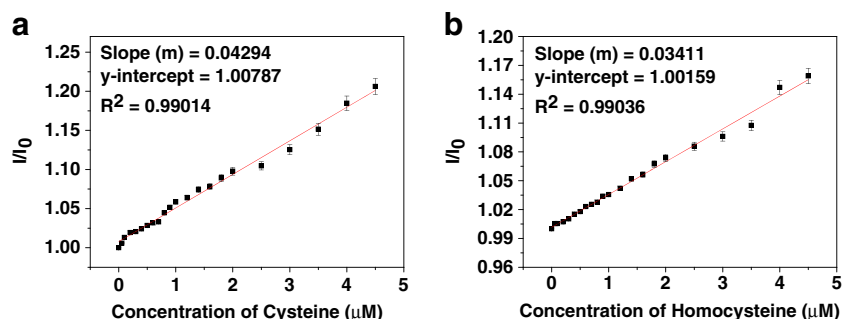
Fig. 8 Time-correlated single photon counting lifetime analysis of gold nanoclusters (Au NCs), Au NC–KI$_3$ system, and Au NC–KI$_3$–cysteine system

spectrum of KI$_3$ [40] and the excitation and emission spectra of Au NCs rules out a mechanism based on an inner filter effect and Förster resonance energy transfer (Fig. 9c). The fluorescence intensity of Au NCs depends on the electropositive nature of the metallic core, and any factors that can decrease the positive nature of the Au(0)–Au(I) core–shell structure decrease the fluorescence intensity [34]. It is well known that I$_3^-$ ions have stronger affinity for Au NCs [41–42], and I$_2$ induces S–S bond formation between BSA components present in different nanoclusters, resulting in the aggregation of Au NCs as evident in the TEM image (Fig. 3d). Thus fluorescence quenching occurs due to energy transfer. The fluorescence lifetime measurements show a difference of 430 ns between Au NCs and quenched Au NCs@KI$_3$. The results suggest that the quenching is static in nature. Here the Cys/Hcy species reduce the S–S bond between BSA in its aggregated form and cause the particles to dissociate back to small Au NCs. Thus the fluorescence lifetime of Au NCs@KI$_3$@Cys/

Fig. 9 a Photographs of the fluorescence response of (a) gold nanoclusters (Au NCs), (b) Au NCs andKI$_3$, (c) Au NCs andKI$_3$ on addition of cysteine, and (d) Au NCs and KI$_3$ on addition of homocysteine (top, solution; bottom, paper strip). **b** UV–visible absorption (Abs.) spectrum of KI$_3$, and excitation (Ex.) and emission (Em.) spectra of Au NCs. X-ray photoelectron spectroscopy 4f spectra of **c** Au NCs, **d** KI$_3$-quenched AuNCs (Au NCs@KI$_3$), and **e** KI$_3$-quenched Au NCs with cysteine (Au NCs@KI$_3$@Cys)

a

Slope (m) = 0.04294
y-intercept = 1.00787
R^2 = 0.99014

b

Slope (m) = 0.03411
y-intercept = 1.00159
R^2 = 0.99036

Fig. 10 **a** The relative intensity of the Au NC–KI_3 system against the concentration of cysteine added to serum samples (concentration of cysteine ranging from 0 to 4.5 μM). **b** The relative intensity of the Au NC–KI_3 system against the concentration of homocysteine added to serum samples (concentration of homocysteine ranging from 0 to 4.5 μM)

Hcy (1.49 μs) returns to that of virgin Au NCs (1.54 μs), with a concomitant obvious change in the size of the Au NCs@KI_3@Cys/Hcy to 7.37 ± 2.5 nm, comparable to that of Au NCs.

The mechanism of quenching and the turn-on response is further confirmed by the deconvoluted X-ray photoelectron spectroscopy spectra of the Au 4*f* electronic state. As shown in Fig. 9c, the binding energies of Au $4f_{7/2}$ and $4f_{5/2}$ are 83.63 eV and 87.02 eV, respectively (see Table S2), which indicates the Au(0) oxidation state, and small peaks at 84.41 eV and 87.73 eV indicate the presence of the Au(I) oxidation state in the A(0)–Au(I) core–shell structure of Au NCs [43–44]. In the KI_3-quenched Au NCs, the binding energies of 83.63 eV and 87.45 eV are attributed to the existence of the Au(0) state, and the absence of other peaks indicates the aggregation of Au NCs. This pristine Cys species stabilize the Au(0)–Au(I) core–shell structure of Au NCs, resulting in the fluorescence of Au NCs being retained to a level greater than that of the parent Au NCs.

Real sample analysis

Real sample analysis was done with serum samples spiked with Cys and Hcy (Fig. 10). The relative intensity shows a linear range from 0 to 4.5 μM (I/I_0 = 0.04294[Cys] + 1.00787 and $I/I0$ = 0.03411[Hcy] + 1.00159). The recovery of the known amount of Cys in serum samples is 93.2–109.5%, whereas that of Hcy is 95.8–113.5%, and the limit of detection is 5 nM for Cys and 8 nM for Hcy. These results suggest the reliability of the Au NCs@KI_3 system for detection of Cys/Hcy in real samples.

Distinction between Cys and Hcy

For the distinctive discrimination of Cys and Hcy, the fluorescence of Au NCs@KI_3 was measured at pH 7.2, and the results prove that Hcy slightly dominates over Cys in turn-on response (see Fig. S5). In addition, the color of the paper strip for both Au NCs@KI_3@Cys and Au NCs–KI_3@Hcy over a pH range from 10.6 to 6.0 indicates that Hcy retains a significant pink color up to pH 6.5, while the color diminishes from pH 8.7 for Cys (see Fig. S6). Studies in this direction taking into consideration the difference in isoelectric points are required to discriminate Cys from Hcy (future studies).

Conclusion

In conclusion, we have developed a Au-NC-mediated fluorescent turn-on sensor for sensitive and selective detection of Hcy/Cys. The method relies on the principle that the fluorescence of Au NCs is quenched by iodine (I_3^-) and recovered by Cys/Hcy, which removes iodine by forming a thiol linkage with the Au NC. The system exhibits high sensitivity and selectivity among other amino acids and glutathione, with a low detection limit. Furthermore, we have demonstrated the fluorescence turn-on response in human serum, which indicates its potential for applications in point-of-care clinical diagnosis.

Compliance with ethical standards

All biological experiments were performed with the approval of the Human Ethics Committee, University of Kerala, Kerala. Informed consent was obtained from all individual participants included in the study

Conflict of interest   The authors declare that they have no competing interests.

Publisher's Note   Springer Nature remains neutral with regard to jurisdictional claims in published maps and institutional affiliations.

References

1. Brattström L, Wilcken DE. Homocysteine and cardiovascular disease: cause or effect? Am J Clin Nutr. 2000;72(2):315–23. https://doi.org/10.1093/ajcn/72.2.315.

2. Sonoda M, Shoji T, Kuwamura Y, Okute Y, Naganuma T, Shima H, et al. Plasma homocysteine and cerebral small vessel disease as possible mediators between kidney and cognitive functions in patients with diabetes mellitus. Sci Rep. 2017;7(1):4382. https://doi.org/10.1038/s41598-017-04515-w.

3. Chung KH, Chiou HY, Chen YH. Associations between serum homocysteine levels and anxiety and depression among children and adolescents in Taiwan. Sci Rep. 2017;7(1):8330. https://doi.org/10.1038/s41598-017-08568-9.

4. Troen AM. The central nervous system in animal models of hyperhomocysteinemia. Prog Neuropsychopharmacol Biol Psychiatry. 2005;29(7):1140–51. https://doi.org/10.1016/j.pnpbp.2005.06.025.

5. Yasar A, Gunduz K, Onur E, Calkan M. Serum homocysteine, vitamin B12, folic acid levels and methylenetetrahydrofolate reductase (MTHFR) gene polymorphism in vitiligo. Dis Markers. 2012;33(2):85–9. https://doi.org/10.3233/DMA-2012-0908.

6. Fratoni V, Brandi ML. B vitamins, homocysteine and bone health. Nutrients. 2015;7(4):2176–92. https://doi.org/10.3390/nu7042176.

7. Guilliams TG. Homocysteine - a risk factor for vascular diseases: guidelines for the clinical practice. J Am Neutraceutical Assoc. 2004;7(1):11–24.

8. Joshi MB, Baipadithaya G, Balakrishnan A, Hegde M, Vohra M, Ahamed R, et al. Elevated homocysteine levels in type 2 diabetes induce constitutive neutrophil extracellular traps. Sci Rep. 2016;6: 36362. https://doi.org/10.1038/srep36362.

9. Ganguly P, Alam SF. Role of homocysteine in the development of cardiovascular disease. Nutr J. 2015;14:6. https://doi.org/10.1186/1475-2891-14-6.

10. Jacobsen DW. Homocysteine and vitamins in cardiovascular disease. Clin Chem. 1998;44(8):1833–43.

11. Eikelboom JW, Lonn E, Genest J Jr, Hankey G, Yusuf S. Homocyst(e)ine and cardiovascular disease: a critical review of the epidemiologic evidence. Ann Intern Med. 1999;131(5):363–75.

12. Ubbink JB. Assay methods for the measurement of total homocyst(e)ine in plasma. Semin Thromb Hemost. 2000;26(3):233–41. https://doi.org/10.1055/s-2000-8468.

13. Yin CX, Xiong KM, Huo FJ, Salamanca JC, Strongin RM. Fluorescent probes with multiple binding sites for the discrimination of Cys, Hcy, and GSH. Angew Chem Int Ed Engl. 2017;56(43):13188–98. https://doi.org/10.1002/anie.20170408.

14. Forman HJ, Zhang H, Rinna A. Glutathione: overview of its protective roles, measurement, and biosynthesis. Mol Aspects Med. 2009;30(1-2):1–12. https://doi.org/10.1016/j.mam.2008.08.006.

15. Liu Y, Yu D, Ding S, Xiao Q, Guo J, Feng G. Rapid and ratiometric fluorescent detection of cysteine with high selectivity and sensitivity by a simple and readily available probe. ACS Appl Mater Interfaces. 2014;6(20):17543–50. https://doi.org/10.1021/am505501d.

16. Wu Q, Zhou J, Wu Y, Yu C, Hao E, Jiao L. Highly selective colorimetric and fluorescent BODIPY dyes for sensing of cysteine and/or homocysteine. New J Chem. 2016;40(2):1387–95. https://doi.org/10.1039/c5nj02346g.

17. Yue Y, Huo F, Li X, Wen Y, Yi T, Salamanca J, et al. pH-dependent fluorescent probe that can be tuned for cysteine or homocysteine. Org Lett. 2017;19(1):82–5. https://doi.org/10.1021/acs.orglett.6b03357.

18. Apyari VV, Arkhipova VV, Isachenko AI, Volkov PA, Dmitrienko SG. Torocheshnikova II. Label-free gold nanoparticle-based sensing of cysteine: new peculiarities and prospects. Sens Actuators B. 2018;260:953–61. https://doi.org/10.1016/j.snb.2018.01.118.

19. Sun J, Yang F, Zhao D, Chen C, Yang X. Integrated logic gate for fluorescence turn-on detection of histidine and cysteine based on Ag/Au bimetallic nanoclusters–Cu^{2+} ensemble. ACS Appl Mater Interfaces. 2015;7(12):6860–6. https://doi.org/10.1021/acsami.5b00434.

20. Rusin O, St. Luce NN, Agbaria RA, Escobedo JO, Jiang S, Warner IM, et al. Visual detection of cysteine and homocysteine. J Am Chem Soc. 2004;126(2):438–9. https://doi.org/10.1021/ja036297t.

21. Yue Y, Huo F, Ning P, Zhang Y, Chao J, Meng X, et al. Dual-site fluorescent probe for visualizing the metabolism of Cys in living cells. J Am Chem Soc. 2017;139(8):3181–5. https://doi.org/10.1021/jacs.6b12845.

22. Liu T, Huo F, Li J, Chao J, Zhang Y, Yin C. An off-on fluorescent probe for specifically detecting cysteine and its application in bioimaging. Sens Actuators B. 2016;237:127–32. https://doi.org/10.1016/j.snb.2016.06.080.

23. Yue Y, Yin C, Huo F, Chao J, Zhang Y. Thiol-chromene click chemistry: a turn-on fluorescent probe for specific detection of cysteine and its application in bioimaging. Sens Actuators B. 2016;223:496–500. https://doi.org/10.1016/j.snb.2015.09.127.

24. Liu T, Huo F, Yin C, Li J, Niu L. A highly selective fluorescence sensor for cysteine/homocysteine and its application in bioimaging. RSC Adv. 2015;5(36):28713–6. https://doi.org/10.1039/c5ra03011k.

25. Li J, Yin C, Zhang Y, Chao J, Huo F. A long wavelength fluorescent probe for biothiols and its application in cell imaging. Anal Methods. 2016;8(37):6748–53. https://doi.org/10.1039/c6ay02150f.

26. Su Y, Qi L, Mu X, Wang M. A fluorescent probe for sensing ferric ions in bean sprouts based on L-histidine-stabilized gold nanoclusters. Anal Methods. 2015;7(2):684–9. https://doi.org/10.1039/c4ay02186j.

27. Xie J, Zheng Y, Ying JY. Protein-directed synthesis of highly fluorescent gold nanoclusters. J Am Chem Soc. 2009;131(3):888–9. https://doi.org/10.1021/ja806804u.

28. Liu H, Li M, Xia Y, Ren X. A turn-on fluorescent sensor for selective and sensitive detection of alkaline phosphatase activity with gold nanoclusters based on inner filter effect. ACS Appl Mater Interfaces. 2017;9(1):120–6. https://doi.org/10.1021/acsami.6b11920.

29. Chang H-C, Ho J-aA. Gold nanocluster-assisted fluorescent detection for hydrogen peroxide and cholesterol based on the inner filter effect of gold nanoparticles. Anal Chem. 2015;87(20):10362–7. https://doi.org/10.1021/acs.analchem.5b02452.

30. Wu Y-T, Shanmugam C, Tseng W-B, Hiseh M-M, Tseng W-L. A gold nanocluster-based fluorescent probe for simultaneous pH and temperature sensing and its application to cellular imaging and logic gates. Nanoscale. 2016;8(21):11210–6. https://doi.org/10.1039/c6nr02341j.

31. Nebu J, Anjali Devi JS, Aparna RS, Abha K, Sony G. Erlotinib conjugated gold nanocluster enveloped magnetic iron oxide nanoparticles–a targeted probe for imaging pancreatic cancer cells. Sens Actuators B. 2018;257:1035–43. https://doi.org/10.1016/j.snb.2017.11.017.

32. Li R, Xu P, Tu Y, Yan J. Albumin-stabilized gold nanoclusters as viable fluorescent probes in non-titrimetric iodometry for the detection of oxidizing analytes. Microchim Acta. 2016;183(1):497–502. https://doi.org/10.1007/s00604-015-1661-y.

33. Zhou M, Zeng C, Chen Y, Zhao S, Sfeir MY, Zhu M, et al. Evolution from the plasmon to exciton state in ligand-protected atomically precise gold nanoparticles. Nat Commun. 2016;7: 13240. https://doi.org/10.1038/ncomms13240.

34. Wu Z, Jin R. On the ligand's role in the fluorescence of gold nanoclusters. Nano Lett. 2010;10(7):2568–73. https://doi.org/10.1021/nl101225f.

35. Lystvet SM, Volden S, Singh G, Yasuda M, Halskau O, Glomm WR. Tunable photophysical properties, conformation and function of nanosized protein-gold constructs. RSC Adv. 2013;3(2):482–95. https://doi.org/10.1039/c2ra22479h.

36. Wang H, Xu C, Zheng C, Xu W, Dong T, Liu K, et al. Facile synthesis and characterization of Au nanoclusters-silica fluorescent composite nanospheres. J Nanomater. 2013;2013:5. https://doi.org/10.1155/2013/972834.

37. Meng H, Yang D, Tu Y, Yan J. Turn-on fluorescence detection of ascorbic acid with gold nanolcusters. Talanta. 2017;165(Suppl C):346–50. https://doi.org/10.1016/j.talanta.2016.12.047.

38. Jung HS, Han JH, Pradhan T, Kim S, Lee SW, Sessler JL, et al. A cysteine-selective fluorescent probe for the cellular detection of cysteine. Biomaterials. 2012;33(3):945–53. https://doi.org/10.1016/j.biomaterials.2011.10.040.

39. Yahia-Ammar A, Sierra D, Mérola F, Hildebrandt N, Le Guével X. Self-assembled gold nanoclusters for bright fluorescence imaging and enhanced drug delivery. ACS Nano. 2016;10(2):2591–9. https://doi.org/10.1021/acsnano.5b07596.

40. Wei YJ, Liu CG, Mo LP. Ultraviolet absorption spectra of iodine, iodide ion and triiodide ion. Spectrosc Spectr Anal. 2005;25(1):86–8.

41. Li R, Xu P, Fan J, Di J, Tu Y, Yan J. Sensitive iodate sensor based on fluorescence quenching of gold nanocluster. Anal Chim Acta. 2014;827(Suppl C):80–5. https://doi.org/10.1016/j.aca.2014.04.013.

42. Chen YM, Cheng TL, Tseng WL. Fluorescence turn-on detection of iodide, iodate and total iodine using fluorescein-5-isothiocyanate-modified gold nanoparticles. Analyst. 2009;134(10):2106–12. https://doi.org/10.1039/b905426j.

43. Huang J, Dai W-L, Fan K. Remarkable support crystal phase effect in Au/FeOx catalyzed oxidation of 1,4-butanediol to γ-butyrolactone. J Catal. 2009;266(2):228–35. https://doi.org/10.1016/j.jcat.2009.06.011.

44. Klyushin AY, Rocha TCR, Havecker M, Knop-Gericke A, Schlogl R. A near ambient pressure XPS study of Au oxidation. Phys Chem Chem Phys. 2014;16(17):7881–6. https://doi.org/10.1039/c4cp00308j.